# Nonfullerene Polymer Solar Cells with 8.5% Efficiency Enabled by a New Highly Twisted Electron Acceptor Dimer

*Ye-Jin Hwang, Haiyan Li, Brett A. E. Courtright, Selvam Subramaniyan, and Samson A. Jenekhe**

Advances in the design and synthesis of nonfullerene electron acceptors in the last few years have enabled progress in developing nonfullerene organic photovoltaics (OPVs) as a promising alternative to fullerene acceptor-based OPV devices.[1–22] The many drawbacks of fullerene-based OPVs, including the small open-circuit voltage ($V_{oc}$), poor light harvesting, high cost, and poor photochemical stability,[1–22] are well known but could ultimately be addressed by exploiting the readily tunable molecular structure of nonfullerene acceptors. However, the power conversion efficiency (PCE) of current nonfullerene polymer solar cells (4%–6%)[1–22] has remained inferior to state of the art fullerene-based devices (8%–10%).[23–28] The major limitations on the efficiency of current nonfullerene OPV devices include the generally much lower short-circuit current density ($J_{sc}$ ) and fill factor (FF) values[1–22] compared to their $PC_{71}BM$ counterparts.[23–28] These limitations are ultimately rooted in the compatibility and morphology of the acceptor molecule/donor polymer blend and the 3D structure of the acceptor. The spherical 3D structure of fullerene acceptors appears to facilitate their universal compatibility with numerous donor polymers,[9,15,29] resulting in the ready formation of interconnected 10–30 nm phase-separated domains with high mobility, isotropic electron transport.[30] Known nonfullerene acceptors are rarely compatible (PCE >3.0%) with more than one donor polymer in OPV devices.[31]

The best performing (PCE >5%) and most promising nonfullerene, small-molecule or oligomer, electron acceptors to date have a $\pi$-conjugated arylene diimide dimer framework.[1–22] These include various perylene diimide (PDI) dimers[10,11,13,19,21] and tetraazabenzodifluoranthene diimide (BFI) dimers.[9,15] A common feature of these most efficient electron acceptor dimers is the steric-induced significant twisting of segments (e.g., PDI or BFI monomeric units) of the molecule, resulting in an overall nonplanar 3D conformation of the dimer.[9–11,13,15,19,21] Such a twisted nonplanar 3D structure of the electron accepting dimer appears to primarily improve morphological compatibility with the electron-donating polymer and thereby significantly enhance charge separation compared to similar planar molecules.[9] In a previous study, we showed that varying the twist angle ($\theta$) between the planar monomeric units of such nonfullerene dimeric acceptors resulted in a large variation of the power conversion efficiency of bulk heterojunction (BHJ) solar cells,[15] suggesting that the twist angle is a potential means to further improve the performance of nonfullerene electron accepting materials in OPVs.

We herein report a new nonfullerene electron acceptor dimer, 2,5-bis(8-(17-phenyl)-7,9,16,18-tetraazabenzodifluoranthene-3,4,12,13-tetracarboxylic acid diimide)-3,4-ethylenedioxythiophene (DBFI-EDOT), with a highly twisted, nonplanar 3D conformation. We show that polymer solar cells incorporating DBFI-EDOT and thiazolothiazole-dithienosilole copolymer (PSEHTT) donor, without using a processing additive, exhibit a record 8.1% PCE with a high open-circuit voltage ($V_{oc}$ = 0.93 V). Furthermore, 6.7% efficient polymer solar cells with a $V_{oc}$ of 0.95 V were achieved when DBFI-EDOT acceptor is paired with the smaller band gap poly(4,8-bis(5-(2-ethylhexyl)thiophen-2-yl)-benzo[1,2-b;4,5-b′]dithiophene-2,6-diyl-alt-(4-(2-ethylhexyl)-3-fluorothieno[3,4-b]thiophene-)-2-carboxylate-2-6-diyl)) (PBDTT-FTTE) donor polymer, demonstrating for the first time that a nonfullerene acceptor can achieve such a high efficiency with two different donor polymers. Combining DBFI-EDOT acceptor with these two different donor polymers (PSEHTT and PBDTT-FTTE) in a ternary blend active layer produced polymer solar cells with a PCE of 8.5%, maximum photocurrent of 15.67 mA $cm^{-2}$, and maximum external quantum efficiency (EQE) of 83%. The present DBFI-EDOT BHJ devices combine maximum EQE values of 78–83% with high $V_{oc}$ of 0.91–0.95 V, and thus have rather low optical band gap energy losses of 0.62–0.77 eV. These results represent an important milestone in the development of nonfullerene OPV materials and devices.

The new electron acceptor dimer, DBFI-EDOT, whose molecular structure is shown in **Figure 1**a, was synthesized by the Stille cross-coupling reaction of the previously reported 8-bromo-17-phenyl-7,9,16,18-tetraazabenzodifluoranthene-3,4,12,13-tetracarboxylic acid diimide (Ph-BFI-Br)[9] with 2,5-bis(trimethylstannyl)-3,4-ethylenedioxythiophene (Scheme S1, Supporting Information). We note that further optimization and scale up of the synthetic procedures would be necessary for the purpose of commercialization. The molecular structure of DBFI-EDOT was confirmed by $^1$H NMR spectroscopy at 0 °C, elemental analysis and high resolution mass spectroscopy. DBFI-EDOT has good solubility (>30 mg $mL^{-1}$) in common organic solvents (e.g., chloroform, chlorobenzene, toluene, etc.) at room temperature, which is suitable for solution-based device fabrication techniques such as spin-coating, inkjet, and roll-to-roll printing. DBFI-EDOT is thermally stable up to 420 °C (5% weight loss) according to thermogravimetric analysis (TGA) (Figure S1, Supporting Information); differential

Dr. Y.-J. Hwang, Dr. H. Li, B. A. E. Courtright, Dr. S. Subramaniyan, Prof. S. A. Jenekhe
Department of Chemical Engineering and Department of Chemistry
University of Washington
Seattle, WA 98195-1750, USA
E-mail: jenekhe@u.washington.edu

DOI: 10.1002/adma.201503801


© 2015 WILEY-VCH Verlag GmbH & Co. KGaA, Weinheim

15214095, 2016, 1, Downloaded from https://onlinelibrary.wiley.com/doi/10.1002/adma.201503801 by Soochow University, Wiley Online Library on [29/01/2024]. See the Terms and Conditions (https://onlinelibrary.wiley.com/terms-and-conditions) on Wiley Online Library for rules of use; OA articles are governed by the applicable Creative Commons License

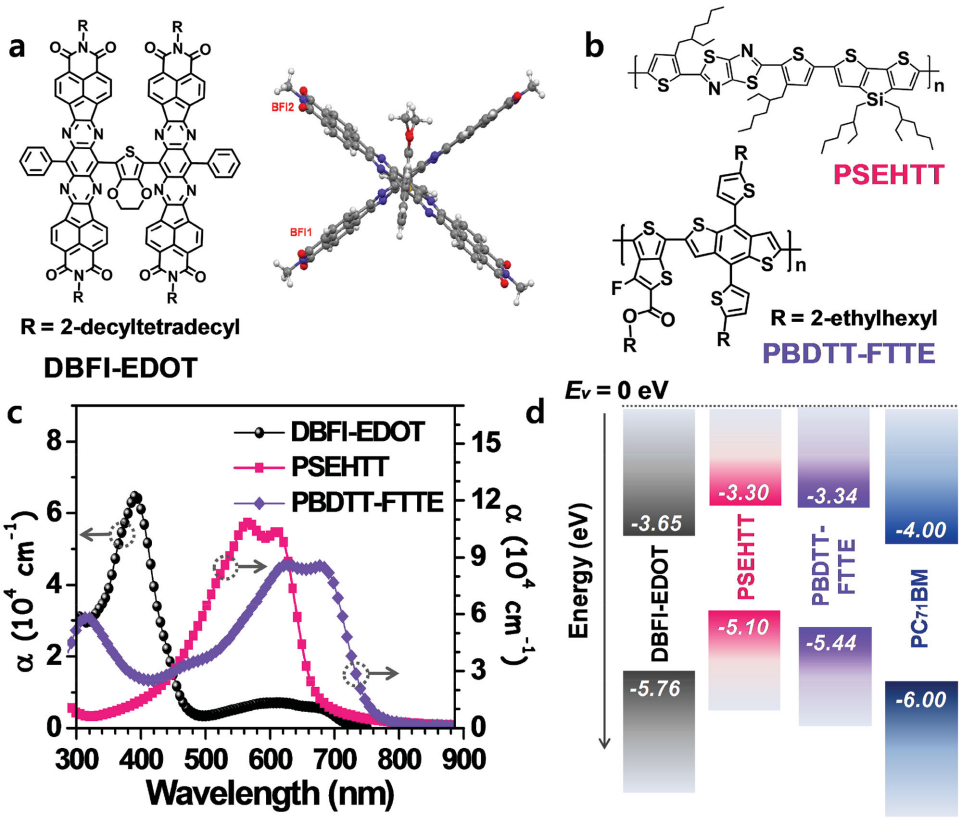


**Figure 1.** a) Molecular structure and side view of the optimized geometry of DBFI-EDOT. b) Molecular structures of PSEHTT and PBDTT-FTTE. c) Thin film optical absorption spectra of DBFI-EDOT, PSEHTT, and PBDTT-FTTE. d) Energy level diagram based on cyclic voltammetry-derived HOMO/LUMO energy levels of DBFI-EDOT, PSEHTT, PBDTT-FTTE, and $PC_{71}BM$.

scanning calorimetry (DSC) scans did not show any thermal transitions in the 20–300 °C range.

The optimized 3D molecular geometry of DBFI-EDOT is shown in Figure 1a and Scheme S2, Supporting Information. Replacing the decyltetradecyl (*R*) groups in DBFI-EDOT with methyl groups simplified the DFT calculations at the B3LYP/6-31G(d) level, giving the geometry optimized structure. Representative geometry parameters (Table S1, Supporting Information) show that DBFI-EDOT has a highly twisted 3D structure with 76° twisting angle ($\theta$) between the two planar monomeric BFI units. Moreover, both BFI units are rotated at larger angles (52°, 55°) with respect to the central EDOT plane in DBFI-EDOT than found in previous thiophene- or selenophene-linked dimers.[9,15] Thus, incorporating a 3,4-ethylenedioxy-2,5-thienylene linker between the BFI units in the dimer framework has dramatically twisted the molecular structure into a nearly perpendicular and more isotropic arrangement.

We used two donor polymers, PSEHTT[32] and PBDTT-FTTE,[26,28] shown in Figure 1b, to evaluate the photovoltaic properties of the new electron acceptor. Both polymers have previously been used to produce high performance BHJ solar cells when paired with $PC_{71}BM$[26,28,32] or with some non-fullerene acceptors.[9,14,33] The thin film absorption spectrum of DBFI-EDOT along with those of the donor polymers are shown in Figure 1c. DBFI-EDOT has an intense high-energy absorption band centered at 391 nm with a maximum absorption coefficient ($\alpha_{max}$) of $6.5 \times 10^4$ $cm^{-1}$, which complements the poor absorption of the donor polymers in this region. An additional broad low-energy absorption band was observed in the 500–730 nm region ($\alpha_{max} = 7.10 \times 10^3$ $cm^{-1}$ at 615 nm), giving rise to an optical band gap ($E_g$) of 1.70 eV. The smaller absorption coefficient of DBFI-EDOT compared to PSEHTT ($E_g = 1.77$ eV, $\alpha_{max} = 1.08 \times 10^5$ $cm^{-1}$ at 580 nm) and PBDTT-FTTE ($E_g = 1.57$ eV, $\alpha_{max} = 8.61 \times 10^4$ $cm^{-1}$ at 645 nm) suggests that acceptor/donor blend ratios greater than 1 would be needed to maximize light harvesting in BHJ devices.

The electronic structures of DBFI-EDOT and the donor polymers (PSEHTT and PBDTT-FTTE) were investigated by using cyclic voltammetry (CV) of thin films. The ferrocene/ferrocenium ($Fc/Fc^+$) reference was used as an external standard, which was assigned an absolute energy of −4.8 eV versus vacuum level.[34] The highest occupied molecular orbital (HOMO)/lowest unoccupied molecular orbital (LUMO) energy levels of DBFI-EDOT obtained from the onset oxidation/reduction potentials of cyclic voltammograms (Figure S2, Supporting Information) are −5.72/−3.65 eV, respectively. The HOMO/LUMO energy levels of PSEHTT and PBDTT-FTTE were −5.10/−3.30 eV and −5.44/−3.34 eV, respectively (Figure S3, Supporting Information). The frontier molecular orbital energies of DBFI-EDOT thus form good energetic offsets with the donor polymers (Figure 1d), providing sufficient driving energy for photoinduced charge transfer in BHJ cells.[35,36]


© 2015 WILEY-VCH Verlag GmbH & Co. KGaA, Weinheim

ADVANCED MATERIALS
www.advmat.de

www.MaterialsViews.com

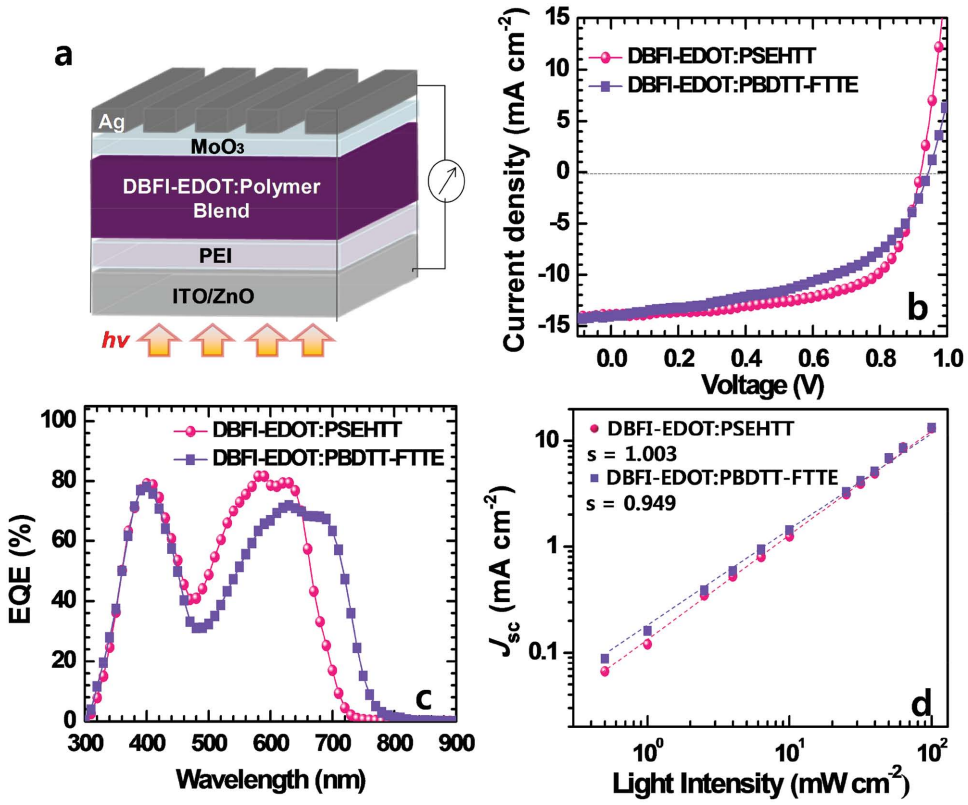


**Figure 2.** a) Schematic of the inverted photovoltaic cell. b) Current density–voltage characteristics, c) external quantum efficiency (EQE) curves, and d) short-circuit current density ($J_{sc}$) versus light intensity ($P_{light}$) data and power-law ($J_{sc} \propto P_{light}^{s}$) fit of DBFI-EDOT:PSEHTT (2:1, wt/wt) and DBFI-EDOT:PBDTT-FTTE (2.5:1, wt/wt) devices.

Note the higher lying LUMO level of DBFI-EDOT compared to $PC_{71}BM$ (–4.0 eV),[23,37] which could facilitate achievement of higher $V_{oc}$ in photovoltaic devices.

We fabricated photodiodes with an inverted structure (ITO/ZnO/PEI/DBFI-EDOT:polymer/$MoO_3$/Ag) (**Figure 2**a) and tested them under 100 mW $cm^{-2}$ air mass 1.5 global (AM 1.5G) solar illumination in ambient air. The DBFI-EDOT:polymer blend active layer was prepared under optimized conditions of spin coating from a chlorobenzene solution and thermal annealing at 175 °C for 10 min in an argon-filled glovebox. The active layer composition was optimized by evaluating DBFI-EDOT:polymer blend ratios from 1.5:1 to 3:1 (wt:wt). We found the optimized compositions to be 2:1 and 2.5:1 for DBFI-EDOT:PSEHTT and DBFI-EDOT:PBDTT-FTTE blends, respectively (Table S2, Supporting Information). Current density versus voltage ($J$–$V$) curves and EQE spectra of the best DBFI-EDOT:polymer blend devices are shown in Figure 2b,c, respectively, and those of the reference $PC_{71}BM$:polymer photodiodes are shown in Figure S4 of the Supporting Information. The photovoltaic parameters, including $J_{sc}$, $V_{oc}$, FF, and PCE, extracted from the $J$–$V$ curves for the DBFI-EDOT:polymer devices, are summarized in **Table 1** along with those of the reference $PC_{71}BM$:polymer photodiodes.

A maximum PCE of 8.10% and an average PCE of 7.85% ± 0.18% were achieved in the optimized DBFI-EDOT:PSEHTT devices (Table 1). Both of these values are by far

**Table 1.** Photovoltaic properties of optimized DBFI-EDOT:polymer binary and ternary blend and $PC_{71}BM$:polymer blend solar cells.

| Blend | $J_{sc}$ [mA $cm^{-2}$] | $V_{oc}$ [V] | FF | PCE [%] | $R_{SH}$ [Ω $cm^2$] | $R_S$ [Ω $cm^2$] |
|---|---|---|---|---|---|---|
| DBFI-EDOT:PSEHTT | 13.82 (13.51 ± 0.34) | 0.93 (0.921 ± 0.005) | 0.63 (0.631 ± 0.004) | 8.10 (7.85 ± 0.18) | 497.13 | 5.74 |
| DBFI-EDOT:PBDTT-FTTE | 13.99 (13.50 ± 0.34) | 0.95 (0.947 ± 0.003) | 0.51 (0.50 ± 0.01) | 6.70 (6.42 ± 0.19) | 286.13 | 10.01 |
| DBFI-EDOT: PSEHTT:PBDTT-FTTE[a)] | 15.67 (15.48 ± 0.27) | 0.91 (0.91 ± 0.004) | 0.60 (0.595 ± 0.011) | 8.52 (8.40 ± 0.09) | 460.93 | 6.02 |
| $PC_{71}BM$:PSEHTT[b)] | 13.18 (12.78 ± 0.26) | 0.67 (0.667 ± 0.003) | 0.64 (0.648 ± 0.007) | 5.62 (5.52 ± 0.09) | 696.19 | 5.40 |
| $PC_{71}BM$:PBDTT-FTTE[b)] | 16.59 (16.22 ± 0.61) | 0.79 (0.784 ± 0.006) | 0.63 (0.606 ± 0.019) | 8.12 (7.67 ± 0.25) | 391.01 | 6.51 |

[a)]Photovoltaic properties of DBFI-EDOT:PSEHTT:PBDTT-FTTE = 2:0.9:0.1 (wt/wt) ternary blend solar cells; [b)]Photovoltaic properties of $PC_{71}BM$-based solar cells fabricated using a processing additive (DIO) (see the Supporting Information). The photovoltaic properties were averaged over 15 devices from 3 different batches.


© 2015 WILEY-VCH Verlag GmbH & Co. KGaA, Weinheim


15214095, 2016, 1, Downloaded from https://onlinelibrary.wiley.com/doi/10.1002/adma.201503801 by Soochow University, Wiley Online Library on [29/01/2024]. See the Terms and Conditions (https://onlinelibrary.wiley.com/terms-and-conditions) on Wiley Online Library for rules of use; OA articles are governed by the applicable Creative Commons License

15214095, 2016, 1, Downloaded from https://onlinelibrary.wiley.com/doi/10.1002/adma.201503801 by Soochow University, Wiley Online Library on [29/01/2024]. See the Terms and Conditions (https://onlinelibrary.wiley.com/terms-and-conditions) on Wiley Online Library for rules of use; OA articles are governed by the applicable Creative Commons License

COMMUNICATION

the best performance seen in nonfullerene polymer solar cells to date. For comparison the reference optimized $PC_{71}BM$:PSEHTT photodiodes, gave the best PCE of 5.62% with an average PCE of 5.52% ± 0.09%. Thus, for the same donor polymer, PSEHTT, the conversion efficiency of the nonfullerene acceptor, DBFI-EDOT, exceeds that of $PC_{71}BM$ by 44%. The enhanced performance of DBFI-EDOT devices is largely a result of the enhanced $V_{oc}$ (0.93 V) compared to the $PC_{71}BM$ cells (0.67 V).

Optimized DBFI-EDOT:PBDTT-FTTE devices had a maximum PCE of 6.70% and an average of 6.42% ± 0.19%. This performance is also among the best for nonfullerene polymer solar cells.[1–22] However, the reference optimized $PC_{71}BM$:PBDTT-FTTE devices fabricated by using 3 vol% of 1,8-diiodooctane (DIO) in chlorobenzene had a maximum PCE of 8.12% and an average of 7.67% ± 0.25%, which are in agreement with previously reported values for this BHJ system.[26,28] Although the $V_{oc}$ of DBFI-EDOT devices with PBDTT-FTTE is larger (0.95 V) compared to that of $PC_{71}BM$ devices (0.79 V), the $J_{sc}$ and FF values of the fullerene devices are much higher. Such differences in $J_{sc}$ and FF values are likely due mainly to a nonoptimal morphology[38] in DBFI-EDOT:PBDTT-FTTE blends.

The EQE spectra of the best DBFI-EDOT:polymer devices are given in Figure 2c, with photoresponses spanning 300–720 nm for PSEHTT and 300–765 nm for PBDTT-FTTE. Note the valleys in the 440–540 nm range of the EQE spectra of both BHJ devices. Observed peak EQE values of 79.1% at 400 nm and 81.6% at 580–650 nm in DBFI-EDOT:PSEHTT devices are the highest observed so far in nonfullerene polymer solar cells and are comparable to the best $PC_{71}BM$:polymer devices.[22–28] Also note that observed photocurrent generation above 700 nm in DBFI-EDOT:PSEHTT comes from excitons in DBFI-EDOT since PSEHTT does not absorb above 700 nm. As with PSEHTT devices, the peak EQE values (78% at 400 nm and 72% at 600–700 nm) in PBDTT-FTTE devices are due to contributions from photoinduced hole and electron transfer processes, respectively. Given the observed high EQE values, optical band gap losses ($E_{loss} = E_g - eV_{oc}$) in the DBFI-EDOT devices, 0.77 eV for PSEHTT and 0.62 eV for PBDTT-FTTE, are remarkably low among high efficiency polymer solar cells.[39,40] Theoretical $J_{sc}$ values calculated from the EQE spectra and the AM 1.5G solar spectrum are 13.07 mA cm$^{-2}$ for PSEHTT device and 13.25 mA cm$^{-2}$ for PBDTT-FTTE device, which are in good agreement with the values obtained from the $J$–$V$ curves.

To gain insight into the charge recombination kinetics in DBFI-EDOT:polymer solar cells, we measured $J_{sc}$ as a function of illumination intensity $P_{light}$ as presented in Figure 2d. Linearity (s = 1) in the power-law dependence ($J_{sc} \propto P_{light}^{s}$) generally indicates weak charge carrier losses due to bimolecular recombination, whereas sublinearity (s < 1) implies significant bimolecular recombination.[41] The observed power-law exponent in DBFI-EDOT:PSEHTT devices (s = 1.003) and DBFI-EDOT:PBDTT-FTTE devices (s = 0.949) means that there is much less bimolecular recombination in the PSEHTT devices than in the PBDTT-FTTE devices. The increased bimolecular recombination in PBDTT-FTTE devices can partly explain their lower fill factor, smaller shunt resistance $R_{SH}$, and larger series resistance $R_S$ compared to the PSEHTT devices (Table 1). The results also imply that the morphology of DBFI-EDOT:PBDTT-FTTE blends is not optimum.

The present photovoltaic results for DBFI-EDOT-based solar cells when taken together with previously reported results for related arylene diimide dimers,[9,15] DBFI-Ar, show a quantifiable relationship between photovoltaic properties and the twist angle $\theta$ of the electron acceptor dimer. A strong dependence of both the $J_{sc}$ and PCE of DBFI-Ar:PSEHTT solar cells on the twist angle is observed (**Figure 3**). A linear relationship between $J_{sc}$ and PCE with twist angle, respectively, is observed except for $\theta < 40°$. If the observed linear trend continues to the maximum possible twist angle of 90°, a PCE of nearly 11% and a $J_{sc}$ close to 18 mA cm$^{-2}$ are anticipated. We note that a detailed theoretical understanding of these observations is currently unavailable. Nevertheless, the observed empirical relationship between the photovoltaic properties and the twist angle of electron acceptor dimers provides a much needed rational strategy in the design of next generation OPV materials.

To further understand the observed trends in $J_{sc}$ and FF values, we measured the bulk charge transport in the DBFI-EDOT:polymer and $PC_{71}BM$:polymer blend active layers, which were similarly prepared as the photovoltaic devices, by using the space-charge-limited current (SCLC) method. The electron mobility was measured in an ITO/ZnO/PEI/active layer/LiF/Al device structure, and the hole mobility was measured in an ITO/PEDOT:PSS/active layer/Au device structure. The current–voltage curves and SCLC fittings of the data are shown in Figure S6 of the Supporting Information and the hole and electron mobilities ($\mu_h$, $\mu_e$) are summarized in **Table 2**. The results show that the hole transport ($\mu_h \approx (0.7–1.0) \times 10^{-3}$ cm$^2$ V$^{-1}$ s$^{-1}$)

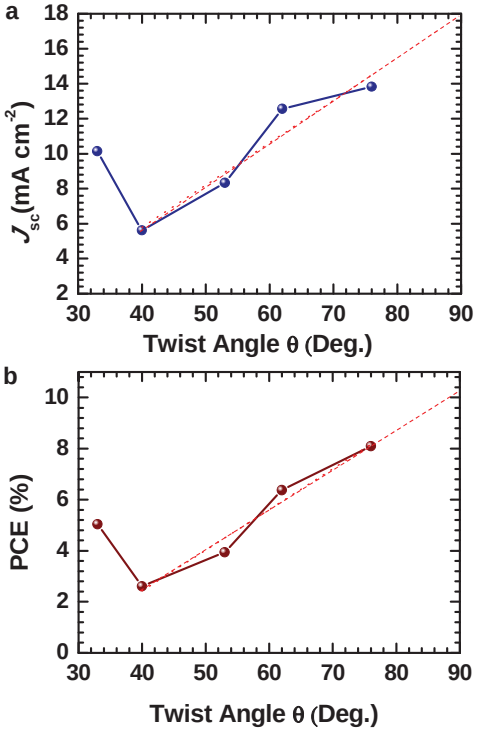


**Figure 3.** a) Dependence of short-circuit current density and b) power conversion efficiency on the twisted angle of dimeric electron acceptors DBFI-Ar. The experimental data points are from the literature values (refs. [9] and [15]) except the present results for $\theta = 76°$. Red dashed line shows linear fit analysis.


© 2015 WILEY-VCH Verlag GmbH & Co. KGaA, Weinheim

**Table 2.** Bulk charge carrier mobilities of DBFI-EDOT:polymer and $PC_{71}BM$:polymer blends under optimized conditions.

| Blend | $\mu_h$ [$cm^2\ V^{-1}\ s^{-1}$] | $\mu_e$ [$cm^2\ V^{-1}\ s^{-1}$] |
|---|---|---|
| DBFI-EDOT:PSEHTT | $7.53 \times 10^{-3}$ | $6.80 \times 10^{-2}$ |
| DBFI-EDOT:PBDTT-FTTE | $6.95 \times 10^{-3}$ | $8.60 \times 10^{-3}$ |
| $PC_{71}BM$:PSEHTT | $7.90 \times 10^{-3}$ | $1.28 \times 10^{-2}$ |
| $PC_{71}BM$:PBDTT-FTTE | $9.75 \times 10^{-3}$ | $1.02 \times 10^{-2}$ |

is comparable in all the blend active layers. Electron mobility is much higher in all the blends due largely to the presence of the PEI interlayer,[42] varying from $8.60 \times 10^{-3}$ $cm^2\ V^{-1}\ s^{-1}$ in DBFI-EDOT:PBDTT-FTTE to $6.80 \times 10^{-2}$ $cm^2\ V^{-1}\ s^{-1}$ in DBFI-EDOT:PSEHTT. The resulting carrier asymmetry ($\mu_h/\mu_e = 0.11$) in the DBFI-EDOT:PSEHTT devices suggests that their further improvement is possible either through a different donor polymer or by means of a suitable anode interlayer.

We used bright-field transmission electron microscopy (BF-TEM) to observe the bulk morphology of DBFI-EDOT:polymer blend films (**Figure 4**). Interconnected phase-separated domains of about 20 nm size are observed in the DBFI-EDOT:PSEHTT blend. In contrast, a less defined phase separation was observed in DBFI-EDOT:PBDTT-FTTE blend film, which is possibly due to the poorer crystallinity of PBDTT-FTTE compared to PSEHTT. X-ray diffraction (XRD) characterization of both the pure polymer films and the DBFI-EDOT:polymer blend films (Figure S7 and Table S4, Supporting Information) confirmed the difference in crystallinity. Mean crystalline domain size ($L_c$)[43] of 8.02 nm and 7.62 nm was observed in pure PSEHTT film and its blend film, respectively, compared with 4.01 nm and 4.55 nm in pure PBDTT-FTTE and its blend, respectively (Figure S7 and Table S4, Supporting Information). These observations are in agreement with the previously discussed lower bulk charge carrier mobilities and higher rate of bimolecular recombination in the DBFI-EDOT:PBDTT-FTTE devices compared to DBFI-EDOT:PSEHTT solar cells.

The above photovoltaic results show that a major limitation of the efficiency of DBFI-EDOT:PSEHTT devices is the small photocurrent, which is due to the narrow optical absorption band of the donor polymer, PSEHTT. One of the effective strategies to enhance the photocurrent of BHJ solar cells is to add a third component to form a ternary blend BHJ system.[44,45] To successfully enhance the photocurrent without disturbing the charge transfer in such ternary blend solar cells, the HOMO/LUMO energy levels of the second donor have to be lower than those of the primary donor polymer but higher than those of the acceptor material.[44,45] We thus fabricated and tested ternary blend (DBFI-EDOT:PSEHTT:PBDTT-FTTE) solar cells under the same conditions as for the binary blend devices. The same total acceptor:donor ratio of 2:1 (wt/wt) found in the PSEHTT binary blends was maintained while the donor composition was varied from PSEHTT:PBDTT-FTTE = 0.9:0.1 (wt/wt) to PSEHTT:PBDTT-FTTE = 0.5:0.5 (wt/wt). The current density versus voltage and EQE curves of the best ternary blend solar cells are shown in **Figure 5**. A maximum PCE of 8.52% and an average of 8.40% ± 0.09% (Table 1) were observed in the ternary blend devices with a composition of DBFI-EDOT:PSEHTT:PBDTT-FTTE = 2:0.9:0.1 wt/wt. The enhanced PCE of the ternary blend, compared to the DBFI-EDOT:PSEHTT binary blend, is due largely to the increased maximum $J_{sc}$ of 15.67 mA $cm^{-2}$ (average $J_{sc}$ = 15.48 ± 0.27 mA $cm^{-2}$) enabled by increased maximum EQE (83%) and the much broader near IR light harvesting that extends to 750 nm in the EQE spectrum (Figure 5b). The $V_{oc}$ (0.91 V) and fill factors (0.60) are slightly decreased in the ternary blend (Table 1) and this decrease can be understood as a consequence of the perturbation of the optimal morphology of the DBFI-EDOT:PSEHTT binary blend films. Indeed, further increase in the amount of PBDTT-FTTE in the ternary blends resulted in a gradual decrease in the PCE due to the gradual decrease of the fill factor whereas the photocurrent and open-circuit voltage were rather similar (Table S3 and Figure S5, Supporting Information). Thus, we expect that the optimal composition of the ternary blend is near the DBFI-EDOT:PSEHTT:PBDTT-FTTE = 2:0.9:0.1 (wt/wt) ratio, although further studies of other donor/acceptor (D/A) ratios may be necessary for a complete understanding of the composition dependence in this ternary blend system.

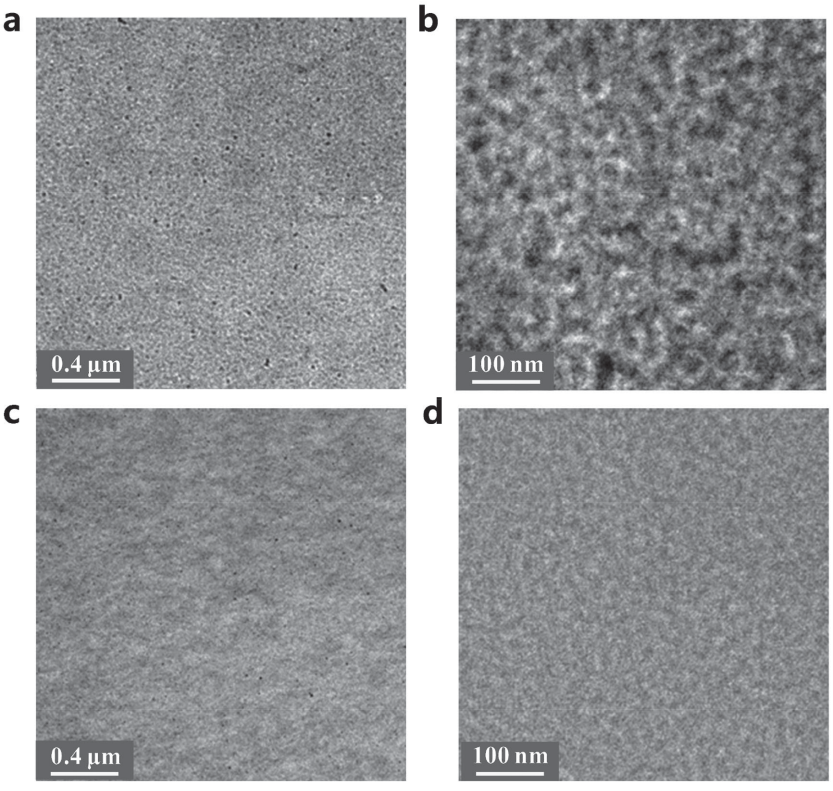


**Figure 4.** a,b) Bright-field (BF)-TEM images of DBFI-EDOT:PSEHTT (2:1 wt/wt) blend film and c,d) DBFI-EDOT:PBDTT-FTTE (2.5:1 wt/wt) blend film.


© 2015 WILEY-VCH Verlag GmbH & Co. KGaA, Weinheim


15214095, 2016, 1, Downloaded from https://onlinelibrary.wiley.com/doi/10.1002/adma.201503801 by Soochow University, Wiley Online Library on [29/01/2024]. See the Terms and Conditions (https://onlinelibrary.wiley.com/terms-and-conditions) on Wiley Online Library for rules of use; OA articles are governed by the applicable Creative Commons License

15214095, 2016, 1, Downloaded from https://onlinelibrary.wiley.com/doi/10.1002/adma.201503801 by Soochow University, Wiley Online Library on [29/01/2024]. See the Terms and Conditions (https://onlinelibrary.wiley.com/terms-and-conditions) on Wiley Online Library for rules of use; OA articles are governed by the applicable Creative Commons License

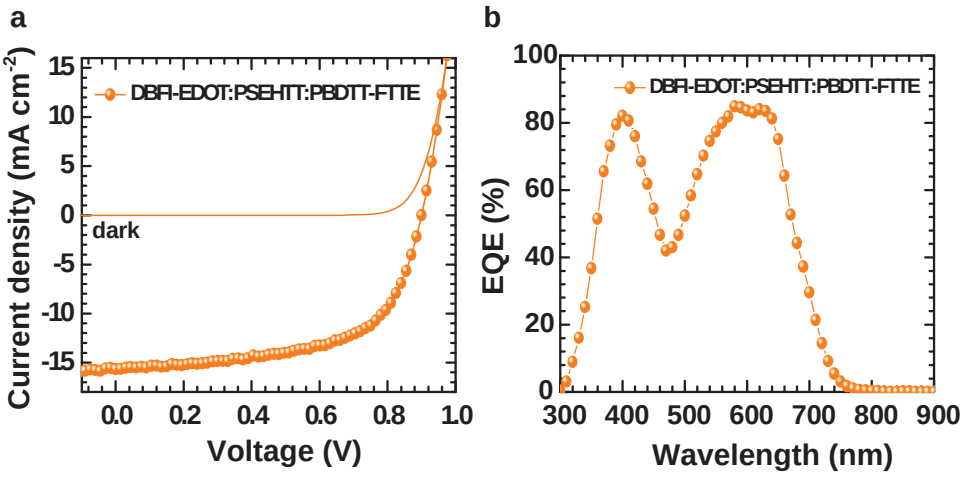


**Figure 5.** a) Current density–voltage characteristics and b) external quantum efficiency (EQE) curves of DBFI-EDOT:PSEHTT:PBDTT-FTTE (2:0.9:0.1, (wt/wt)) ternary blend devices.

In conclusion, we have successfully demonstrated fullerene-free and processing additive-free polymer solar cells with power conversion efficiency (8.1%–8.5%) comparable to some of the best $PC_{71}BM$/polymer devices by using a new electron acceptor dimer, DBFI-EDOT. Success of DBFI-EDOT demonstrates that the twisting angle between building block elements in a molecule is a promising rational design strategy toward more efficient OPV electron acceptors. Observed high $V_{oc}$ (0.91–0.95 V), high quantum efficiency (≈80%), and rather low optical band gap energy loss (0.62–0.77 eV) in DBFI-EDOT BHJ devices offer opportunity for deepening understanding of OPV device physics beyond fullerene limits.[39,40] The finding that efficiency (8.1%) of DBFI-EDOT:PSEHTT devices exceeds that of the corresponding $PC_{71}BM$:PSEHTT photodiodes by 44% suggests that further advances in materials and device engineering will enable nonfullerene OPVs to surpass current fullerene-based solar cells. DBFI-EDOT is the first nonfullerene electron acceptor to achieve high performance (>6.7%) BHJ solar cells with two different donor polymers. The present ternary blend (DBFI-EDOT:PSEHTT:PBDTT-FTTE) solar cells demonstrate the potential to use this strategy to further enhance the performance of nonfullerene OPVs.

## Experimental Section

*Materials*: PSEHTT ($M_n$ = 33.9 kDa, PDI = 3.9) was synthesized according to the known procedure.[32] PBDTT-FTTE ($M_n$ > 25 kDa, PDI = 1.8–2.2) and $PC_{71}BM$ were purchased from Solarmer Energy, Inc. and American Dye Source, Inc. (Quebec, Canada), respectively, and were used as received without further purification.

Synthesis of 2,5-bis(8-(17-phenyl)-7,9,16,18-tetraazabenzodifluoranthene-3,4,12,13-tetracarboxylic acid diimide)-3,4-ethylenedioxythiophene (DBFI-EDOT): Under argon, Ph-BFI-Br (200 mg, 0.14 mmol), 2,5-bis(trimethylstannyl)-3,4-ethylenedioxythiophene (32.8 mg, 0.07 mmol), $Pd_2(dba)_3$ (9 mg), and P(o-Tol)$_3$ (12 mg) were transferred into a Schlenk tube and dissolved in 14 mL of degassed toluene. The mixture was heated to reflux and kept stirring for 72 h. After removing all the volatile materials, the solid residue was purified by chromatography with chloroform and a few drops of methanol as the eluent. The product was isolated as a green solid. Yield: 101 mg, 52.1%. $^1$H NMR ($CDCl_3$, 0 °C, 500 MHz): $\delta$ = 9.25 (br, 4H), 8.75 (s, 4H), 8.65 (s, 4H), 8.53 (s, 4H), 7.97 (br, 4H), 7.80 (m, 6H), 4.14 (d, 8H), 2.77 (br, 10H), 2.39 (br, 4H), 1.20 (s, 4H), 1.4-1.1 (m, 150H), 0.83 (m, 24H). Elemental analysis calcd for $C_{182}H_{226}N_{12}O_8S$: C 78.80%, H 8.21%, N 6.06%; found C 79.26%, H 8.00%, N 5.99%. HRMS (m/z): [M]+ calcd. for $C_{182}H_{226}N_{12}O_{10}S$, 2772.73; found, 2773.39.

*Characterization*: $^1$H NMR spectra were recorded on a Bruker AV500 at 500 MHz using deuterated chloroform ($CDCl_3$) as the solvent. Mass spectra were obtained from Bruker AutoFlex II matrix-assisted LASER desorptionionization–time of flight mass spectrometer (MALDI-TOF) using benzo[$\alpha$]pyrene as a matrix recorded in a (+)-reflector mode. TGA of the dimer molecules was conducted on a TA Instrument model Q50 TGA. A heating rate of 10 °C min$^{-1}$ under flowing $N_2$ was used with runs conducted from room temperature to 600 °C. DSC analysis was performed on a TA Instruments Q100 under flowing $N_2$ at a heating rate of 20 °C min$^{-1}$. The second-heating and corresponding cooling DSC scans were reported.

CV experiments were done on an EG&G Princeton Applied Research potentiostat/galvanostat (model 273A) in an electrolyte solution of 0.1 M tetrabutylammonium hexafluorophosphate ($Bu_4NPF_6$) in acetonitrile at a scan rate of 50 m V$^{-1}$ s$^{-1}$. Platinum (Pt) wires were used as counter and working electrodes, and Ag/Ag+ (Ag in 0.1 M $AgNO_3$ solution, Bioanalytical System, Inc.) was used as a reference electrode. Ferrocene/ferrocenium ($Fc/Fc^+$) was used as an external standard, and the reference potential was converted to the saturated calomel electrode (SCE) scale. Each sample for CV was prepared by dip-coating the solution in chloroform onto Pt wires.

Optical absorption spectra were measured on a Perkin–Elmer model Lambda 900 UV/vis/near-IR spectrophotometer. Solution and solid-state absorption spectra were obtained from dilute ($10^{-6}$ M) solutions in chloroform and as thin films on glass substrates, respectively.

XRD patterns were obtained from a Bruker F8 powder XRD with a Cu K$\alpha$ radiation as the X-ray source, and the film samples were prepared by drop-casting of highly concentrated polymer solutions (30 mg mL$^{-1}$) in chlorobenzene onto glass substrates and followed by annealing on a hot plate at 175 °C for 10 min. The mean size of the crystalline domains ($L_c$) of the polymers was calculated from the lamellar peaks using the Scherrer equation,[43] $L_c = K\lambda/\beta \cos\theta$, where $K$ is shape factor (0.9), $\lambda$ is X-ray wavelength (1.54 Å), and $\beta$ is the full-width-at-half-maximum (fwhm) in radian. The peak center and the fwhm were obtained by fitting the lamellar peak using Gaussian function in Origin software.

BF-TEM images were acquired on an FEI Tecnai G2 F20 TEM at 200 kV accelerating voltage and acquired with a CCD camera and recorded with Gatan Digital Micrograph software with proper exposure time (0.1 s). The TEM images were slightly defocused to enhance the phase contrast.


© 2015 WILEY-VCH Verlag GmbH & Co. KGaA, Weinheim

The sample films were spin-casted on top of ITO/PEDOT:PSS substrates and peeled off by putting the samples in water. A peeled-off film was deposited on a TEM grid (Electron Microscopy Sciences, Inc.) and dried overnight in a vacuum oven.

*Nonfullerene OPV Device Fabrication*: ITO glass substrates were cleaned sequentially in ultrasonic baths with acetone and isopropyl alcohol for 20 min, dried using nitrogen gas, and stored in a glove box. Each ITO glass substrate was UV-ozone treated for 5 min right before coating the ZnO layer. The ZnO precursor solution (5 g of zinc acetate, 0.14 g of ethanolamine and 5 mL of 2-methoxyethanol) was spin-coated onto the ITO glass at 5000 rpm for 40 s, annealed at 250 °C on a hot plate in air for 1 h to make ≈20 nm thick ZnO layer. A 0.05 wt% polyethylenimine (PEI, $M_w \approx 25\,000$, Aldrich 408727) in 2-methoxyethanol solution was spin-coated onto the ZnO layer and dried at 110 °C on a hot plate in air for 10 min and the glass/ITO/ZnO/PEI substrate was transferred into an argon-filled glove box. Each active layer was spin-coated from the acceptor:polymer blend solution in chlorobenzene solvent. The solution for the DBFI-EDOT:PSEHTT blend (2:1 wt/wt) active layer was prepared from the DBFI-EDOT (20 mg $mL^{-1}$) and PSEHTT (10 mg $mL^{-1}$) solutions in chlorobenzene, mixed and stirred overnight at room temperature in the glove box. The solution for DBFI-T:PBDTT-FTTE blend (2.5:1 wt/wt) active layer was prepared from the DBFI-EDOT (20 mg $mL^{-1}$) and PBDTT-FTTE (20 mg $mL^{-1}$) solutions in chlorobenzene, mixed and stirred overnight at room temperature in the glove box. The solution for DBFI-EDOT:PSEHTT:PBDTT-FTTE = 2:0.9:0.1(wt/wt) ternary blend active layer was prepared from the DBFI-EDOT (20 mg $mL^{-1}$), PSEHTT (10 mg $mL^{-1}$), and PBDTT-FTTE (20 mg $mL^{-1}$) solutions in chlorobenzene, mixed, and stirred overnight at room temperature in the glove box. Each active layer was spin-coated at 1000 rpm for 30 s. After spin-coating, the blend film was thermally annealed at 175 °C on a hot plate in the glove box for 10 min. All the active layers had thicknesses of 110 ± 5 nm. $MoO_3$ (7.5 nm) and Ag anode (100 nm) were thermally deposited onto the active layer. Five pixels, each with an active area of 4 $mm^2$, were fabricated per ITO substrate.

*OPV Device Characterization*: The photovoltaic cells were tested under AM 1.5G solar illumination at 100 mW $cm^{-2}$ in ambient air using a Solar Simulator (model 16S, Solar Light Co., Philadelphia, PA) with a 200W Xenon Lamp Power Supply (Model XPS 200, Solar Light Co., Philadelphia, PA) calibrated by NREL certified Si photodiode (Model 1787–04, Hamamatsu Photonics K.K., Japan) and a HP4155A semiconductor parameter analyzer (Yokogawa Hewlett-Packard, Japan). After the *J–V* measurement, the EQE was measured by using a solar cell quantum efficiency measurement system (Model QEX10, PV Measurements, Inc., Boulder, CO) with a 2 $mm^2$ (2 × 1 mm) size masked incident light source and TF Mini Super measurement apparatus for multiple devices in a single substrate. The EQE system was calibrated with a Si photodiode before each measurement.

*Space-Charge-Limited Current Measurement*: Current–voltage (*J–V*) characteristics of the SCLC devices were measured by using a HP4155A semiconductor parameter analyzer (Yokogawa Hewlett-Packard, Tokyo). The carrier mobility was extracted by fitting the *J–V* curves in the near quadratic region according to the modified Mott–Gurney equation. The SCLC device structures for electron-only and hole-only measurements were ITO/ZnO/PEI/active-layer/LiF/Al and ITO/PEDOT:PSS/active-layer/Au, respectively. Each active blend solution in chlorobenzene was spin-coated at 900 rpm for 30 s. All the active layers had thicknesses of 125 ± 5 nm. After spin-coating, the film was thermally annealed at 175 °C on a hot plate in the glove box for 10 min followed by thermal vacuum deposition of LiF (1 nm)/Al (100 nm) or Au (40 nm).

## Supporting Information

Supporting Information is available from the Wiley Online Library or from the author.

## Acknowledgements

Y.-J.H. and H.L. contributed equally to this work. This work was supported by the NSF (CBET-1435912 and DMR-1409687) and in part by the Office of Naval Research (ONR) (N00014-11-1-0317).

Received: August 5, 2015
Revised: September 16, 2015
Published online: October 29, 2015

[1] P. Sonar, J. P. F. Lin, K. L. Chan, *Energy Environ. Sci.* **2011**, *4*, 1558.
[2] C. H. Woo, T. W. Holcombe, D. A. Unruh, A. Sellinger, J. M. J. Frechet, *Chem. Mater.* **2010**, *22*, 1673.
[3] E. Ahmed, G. Ren, F. S. Kim, E. C. Hollenbeck, S. A. Jenekhe, *Chem. Mater.* **2011**, *23*, 4563.
[4] J. E. Anthony, *Chem. Mater.* **2011**, *23*, 583.
[5] Y. Zhou, L. Ding, K. Shi, Y. Z. Dai, N. Ai, J. Wang, J. Pei, *Adv. Mater.* **2012**, *24*, 957.
[6] P. E. Hartnett, A. Timalsina, H. S. S. Ramakrishna Matte, N. Zhou, X. Guo, W. Zhao, A. Facchetti, R. P. H. Chang, M. C. Hersam, M. R. Wasielewski, T. J. Marks, *J. Am. Chem. Soc.* **2014**, *136*, 16345.
[7] J. T. Bloking, T. Giovenzana, A. T. Higgs, A. J. Ponec, E. T. Hoke, K. Vandewal, S. Ko, Z. Bao, A. Sellinger, M. D. McGehee, *Adv. Energy Mater.* **2014**, *4*, 1301426.
[8] T. V. Pho, F. M. Toma, B. J. Tremolet de Villers, S. Wang, N. D. Treat, N. D. Eisenmenger, G. M. Su, R. C. Coffin, J. D. Douglas, J. M. J. Fréchet, G. C. Bazan, F. Wudl, M. L. Chabinyc, *Adv. Energy Mater.* **2014**, *4*, 1301007.
[9] H. Li, T. Earmme, G. Ren, A. Saeki, S. Yoshikawa, N. M. Murari, S. Subramaniyan, M. J. Crane, S. Seki, S. A. Jenekhe, *J. Am. Chem. Soc.* **2014**, *136*, 14589.
[10] Y. Zhong, M. T. Trinh, R. Chen, W. Wang, P. P. Khlyabich, B. Kumar, Q. Xu, C. Y. Nam, M. Y. Sfeir, C. Black, M. L. Steigerwald, Y. L. Loo, S. Xiao, F. Ng, X. Y. Zhu, C. Nuckolls, *J. Am. Chem. Soc.* **2014**, *136*, 15215.
[11] X. Zhang, C. Zhan, J. Yao, *Chem. Mater.* **2015**, *27*, 166.
[12] S. Holliday, R. S. Ashraf, C. B. Nielsen, M. Kirkus, J. A. Röhr, C. H. Tan, E. Collado-Fregoso, A. C. Knall, J. R. Durrant, J. Nelson, I. McCulloch, *J. Am. Chem. Soc.* **2015**, *137*, 898.
[13] J. Zhao, Y. Li, H. Lin, Y. Liu, K. Jiang, C. Mu, T. Ma, J. Y. L. Lai, H. Hu, D. Yu, H. Yan, *Energy Environ. Sci.* **2015**, *8*, 520.
[14] Y. Lin, Z. G. Zhang, H. Bai, J. Wang, Y. Yao, Y. Li, D. Zhu, X. Zhan, *Energy Environ. Sci.* **2015**, *8*, 610.
[15] H. Li, Y. J. Hwang, B. A. E. Courtright, F. N. Eberle, S. Subramaniyan, S. A. Jenekhe, *Adv. Mater.* **2015**, *27*, 3266.
[16] Y. Liu, L. Zhang, H. Lee, H. W. Wang, A. Santala, F. Liu, Y. Diao, A. L. Briseno, T. P. Russell, *Adv. Energy, Mater.* **2015**, *5*, 1500195.
[17] H. Bai, Y. Wang, P. Cheng, J. Wang, Y. Wu, J. Hou, X. Zhan, *J. Mater. Chem. A* **2015**, *3*, 1910.
[18] O. K. Kwon, J. H. Park, D. W. Kim, S. K. Park, S. Y. Park, *Adv. Mater.* **2015**, *27*, 1951.
[19] L. Ye, K. Sun, W. Jiang, S. Zhang, W. Zhao, H. Yao, Z. Wang, J. Hou, *ACS Appl. Mater. Interfaces* **2015**, *7*, 9274.
[20] Y. Cai, L. Huo, X. Sung, D. Wei, M. Tang, Y. Sun, *Adv. Energy Mater.* **2015**, *5*, 1500032.
[21] S. Rajaram, R. Shivanna, S. K. Kandappa, K. S. Narayan, *J. Phys. Chem. Lett.* **2012**, *3*, 2405.
[22] Y. Fang, A. K. Pandey, A. M. Nardes, N. Kopidakis, P. L. Burn, P. Meredith, *Adv. Energy Mater.* **2013**, *3*, 54.
[23] Z. He, C. Zhong, S. Su, H. Wu, Y. Cao, *Nat. Photonics* **2012**, *6*, 591.
[24] G. Li, R. Zhu, Y. Yang, *Nat. Photonics* **2012**, *6*, 153.


© 2015 WILEY-VCH Verlag GmbH & Co. KGaA, Weinheim


15214095, 2016, 1, Downloaded from https://onlinelibrary.wiley.com/doi/10.1002/adma.201503801 by Soochow University, Wiley Online Library on [29/01/2024]. See the Terms and Conditions (https://onlinelibrary.wiley.com/terms-and-conditions) on Wiley Online Library for rules of use; OA articles are governed by the applicable Creative Commons License

[25] X. Guo, N. Zhou, S. J. Lou, J. Smith, D. B. Tice, J. W. Hennek, R. P. Ortiz, J. T. López Navarrete, S. Li, J. Strzalka, L. X. Chen, R. P. H. Chang, A. Facchetti, T. J. Marks, *Nat. Photonics* **2013**, *7*, 825.
[26] S. H. Liao, H. J. Jhuo, Y. S. Cheng, S. A. Chen, *Adv. Mater.* **2013**, *25*, 4766.
[27] C. J. Brabec, S. Gowrisanker, J. J. M. Halls, D. Laird, S. Jia, S. P. Williams, *Adv. Mater.* **2010**, *22*, 3839.
[28] C. Cui, W. Y. Wong, Y. Li, *Energy Environ. Sci.* **2014**, *7*, 2276.
[29] B. M. Savoie, A. Rao, A. A. Bakulin, S. Gelinas, B. Movaghar, R. H. Friend, T. J. Marks, M. A. Ratner, *J. Am. Chem. Soc.* **2014**, *136*, 2876.
[30] J. Roncali, P. Leriche, A. Cravino, *Adv. Mater.* **2007**, *19*, 2045.
[31] H. Li, T. Earmme, S. Subramaniyan, S. A. Jenekhe, *Adv. Energy Mater.* **2015**, *5*, 1402041.
[32] S. Subramaniyan, H. Xin, F. S. Kim, S. Shoaee, J. R. Durrant, S. A. Jenekhe, *Adv. Energy Mater.* **2011**, *1*, 854.
[33] Y. J. Hwang, B. A. E. Courtright, A. S. Ferreira, S. H. Tolbert, S. A. Jenekhe, *Adv. Mater.* **2015**, *27*, 4578.
[34] V. V. Pavlishchuk, A. W. Addison, *Inorg. Chim. Acta* **2000**, *298*, 97.
[35] A. J. Heeger, *Adv. Mater.* **2014**, *26*, 10.
[36] G. Ren, C. W. Schlenker, E. Ahmed, S. Subramaniyan, S. Olthof, A. Kahn, D. S. Ginder, S. A. Jenekhe, *Adv. Funct. Mater.* **2013**, *23*, 1238.
[37] M. M. Wienk, J. M. Kroon, W. J. H. Verhees, J. Knol, J. C. Hummelen, P. A. van Hal, R. A. J. Janssen, *Angew. Chem. Int. Ed.* **2003**, *42*, 3371.
[38] N. E. Jackson, B. M. Savoie, T. J. Marks, L. X. Chen, M. A. Ratner, *J. Phys. Chem. Lett.* **2015**, *6*, 77.
[39] W. Li, K. H. Hendriks, A. Furlan, M. M. Wienk, R. A. J. Janssen, *J. Am. Chem. Soc.* **2015**, *137*, 2231.
[40] M. Wang, H. Wang, T. Yokoyama, X. Liu, Y. Huang, Y. Zhang, T. Q. Nguyen, S. Aramaki, G. C. Bazan, *J. Am. Chem. Soc.* **2014**, *136*, 12576.
[41] P. Schilinsky, C. Waldauf, C. J. Brabec, *Appl. Phys. Lett.* **2002**, *81*, 3885.
[42] Y. Zhou, C. Fuentes-Hernandez, J. Shim, J. Meyer, A. J. Giordano, H. Li, P. Winget, T. Papadopoulos, H. Cheun, J. Kim, M. Fenoll, A. Dindar, W. Haske, E. Najafabadi, T. M. Khan, H. Sojoudi, S. Barlow, S. Graham, J. L. Brédas, S. R. Marder, A. Kahn, B. Kippelen, *Science* **2012**, *336*, 327.
[43] A. L. Patterson, *Phys. Rev.* **1939**, *56*, 978.
[44] T. Ameri, P. Khoram, J. Min, C. J. Brabec, *Adv. Mater.* **2013**, *25*, 4245.
[45] Y. J. Hwang, B. A. E. Courtright, S. A. Jenekhe, *MRS Commun.* **2015**, *5*, 229.


© 2015 WILEY-VCH Verlag GmbH & Co. KGaA, Weinheim


15214095, 2016, 1, Downloaded from https://onlinelibrary.wiley.com/doi/10.1002/adma.201503801 by Soochow University, Wiley Online Library on [29/01/2024]. See the Terms and Conditions (https://onlinelibrary.wiley.com/terms-and-conditions) on Wiley Online Library for rules of use; OA articles are governed by the applicable Creative Commons License